ACS NANO
Cite This: ACS Nano 2019, 13, 13176−13184
www.acsnano.org

ARTICLE

Direct-Ink-Write 3D Printing of Hydrogels into Biomimetic Soft Robots

Yin Cheng, Kwok Hoe Chan, Xiao-Qiao Wang, Tianpeng Ding, Tongtao Li, Xin Lu, and Ghim Wei Ho*

Department of Electrical and Computer Engineering, National University of Singapore, 4 Engineering Drive 3, Singapore 117583

Supporting Information

ABSTRACT: Hydrogels are promising starting materials for biomimetic soft robots as they are intrinsically soft and hold properties analogous to nature's organic parts. However, the restrictive mold-casting and post-assembly fabrication alongside mechanical fragility impedes the development of hydrogel-based soft robots. Herein, we harness biocompatible alginate as a rheological modifier to manufacture 3D freeform architectures of both chemically and physically cross-linked hydrogels using the direct-ink-write (DIW) printing. The intrinsically hydrophilic polymer network of alginate allows the preservation of the targeted functions of the host hydrogels, accompanied by enhanced mechanical toughness. The integration of free structures and available functionalities from diversified hydrogel family renders an enriched design platform for bioinspired fluidic and stimulus-activated robotic prototypes from an artificial mobile tentacle, a bioengineered robotic heart with beating−transporting functions, and an artificial tendril with phototropic motion. The design strategy expands the capabilities of hydrogels in realizing geometrical versatility, mechanical tunability, and actuation complexity for biocompatible soft robots.

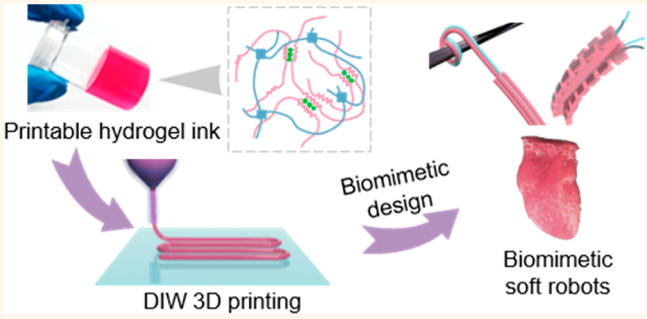

KEYWORDS: *direct-ink-write printing, hydrogels, mechanical strengthening, biomimetic soft robots*

Soft robotics has aroused intense research interest in the past few years, as it promises the integration of motion agility, human interaction safety, and adaptability to unstructured environments.[1−9] Such features greatly facilitate the realization of robotic counterparts that mimic those sophisticated systems in nature, with examples ranging from an artificial flytrap[10] and nocturnal flower[11] to a soft robotic ray[12] and a soft electronic fish.[13] The building of soft robots fundamentally relies on the exploitation of materials with compliance similar to that of soft biological matter. Hydrogel materials have emerged in the realm of biomimetic soft robotics,[14−24] as they not only possess intrinsic softness but also exhibit other favorable properties held by nature's organic parts, like stretchability, biocompatibility, permeability, and stimuli adaptability, owing to their diversified family. These imperative properties can help better imitate the diverse features mandatory for the nature-inspired robotic systems. However, currently, the pervasive application of hydrogel-based soft robots is still hampered by two challenges. For one thing, conventional hydrogels usually show limited mechanical robustness and are liable to permanent damage.[25] For another, the construction of hydrogel-based robots typically depends on custom-designed molds and laborious post-assembly,[15,26−29] which is time-consuming for prototyping and design iteration. More importantly, such mold-casting technique is usually confined to the construction of 2D or simple 3D architectures, such as the typical bilayer design with a restrictive uniaxial bending.[28−30] The limited geometry inevitably hinders further enrichment and complexity of the robotic motion.

In order for the soft robots to assimilate functionalities similar to those of living organisms, they are to be fabricated in a different manufacturing paradigm rather than mechanical assembly of elementary building blocks, as in the case of rigid-body robots. In this respect, 3D printing represents an efficient fabricating method to construct arbitrary, delicate, and continuous structures.[31] Pre-cross-linking the hydrogel precursors can effectively increase the viscosity of the resultant solution to allow the printing;[32,33] however, mechanical strengthening is usually not fulfilled for the final printed hydrogel. Nanoclays and silica particles,[34−38] as non-homogeneous thickening materials, have also been employed to give the hydrogel precursor ink the desired rheological properties for printing. Nevertheless, the introduction of such materials with properties distinctly different than hydrogels can compromise the hydrogel-related features, such as the softness,

Received: August 4, 2019
Accepted: October 18, 2019
Published: October 18, 2019

DOI: 10.1021/acsnano.9b06144
ACS Nano 2019, 13, 13176−13184

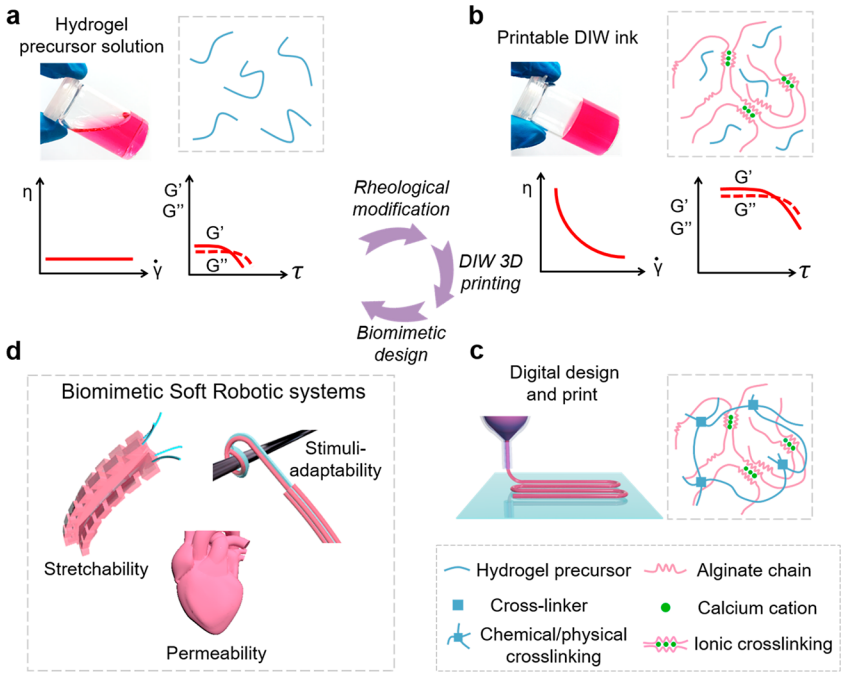

Figure 1. Schematic illustration of DIW 3D printing hydrogels into biomimetic soft robots. (a) Hydrogel precursor solution photo (AAM as an example here) with the composition diagram and typical water-like rheological behavior. (b) Printable DIW ink photo (AAM DIW ink as an example here) with the composition diagram and typical gel-like rheological behavior after rheological modification. (c) Digital design and print of DIW ink (schematic) and the composition diagram after hydrogel curing. (d) Biomimetic soft robotic systems (schematic) including an artificial tentacle, a bioengineered robotic heart, and an artificial tendril.

transparency, and responsiveness. In addition, very few of these works focus on the design and engineering of hydrogel-based soft robots. For the application of hydrogels in biomimetic soft robotics, the rheological tuning materials should not only hold the desirable properties specific to hydrogels, like hydrophilicity, softness, and permeability, but also work at a low dosage to retain the targeted functions of the host hydrogels, such as stimuli-responsiveness. Also, it is important that the rheological modifier exhibits well-proven biocompatibility and low toxicity for the soft robots to be used in scenarios where close interaction with the human body and biomedical applications are involved. In general, there is still a lack of facile and versatile manufacturing schemes that can enable the fast design of biomimetic soft robots from hydrogel materials with desired sophistication in architecture and robotic performance.

Herein, faced by the shortcomings of existing approaches, we utilize a biocompatible alginate-based naturally occurring ionically percolating network as a versatile rheological modifier to rapidly manufacture 3D topologies using the direct-ink-write (DIW) 3D printing of both chemically and physically cross-linked classes of functional hydrogels. The intrinsic hydrophilic polymer network of alginate at a low addition amount (~6 wt %) allows the preservation of the valuable properties of the functional hydrogel materials, accompanied by substantially enhanced mechanical toughness. Equipped with a compatible support printing method, the DIW 3D printing permits complex architectures of the modified hydrogels involving 3D structures with hollow and suspended features. The sophisticated geometry design enabled by the additive printing, unified with the availability of multifaceted functions inherited from the host hydrogels, provides a rich platform for the freeform design and manufacturing of hydrogel-based biomimetic soft robots. We demonstrate a series of representative bioinspired fluidic and stimulus-activated robotic prototypes with intricate functionalities, including a hydraulically controlled artificial tentacle based on the stretchability of polyacrylamide (PAM), a bioengineered robotic heart based on the softness, permeability and biocompatibility of poly(vinyl alcohol) (PVA), and an artificial tendril based on the flexibility and thermoresponsiveness of poly(*N*-isopropylacrylamide) (PNIPAM). As such, the typical mold-casted restrictive geometry with a single motion type is contrasted by 3D-printed elaborate shapes with augmented complexity in movement manipulation. The accessibility of such simple nonintrusive mild gelation modification methodology bridges the design engineering challenge and the application realization to create geometrically versatile, mechanically compliant, and biocompatible soft devices and robots.

RESULTS AND DISCUSSION

Concept of DIW 3D Printing Hydrogels into Biomimetic Soft Robots. Figure 1 shows the schematic description of printing hydrogels into soft robots. The precursor solution (Figure 1a) of targeted hydrogels with desired properties typically exhibits a water-like fluidity, indicated by a constant low viscosity (η) along a wide shear rate ($\dot{\gamma}$), and low storage modulus (G') and shear yield stress (τ_γ, the crossover point of G' and loss modulus G''). After introducing an appropriate dosage of dynamically reversible ionic-cross-linking network composed of alginate polymer and calcium cations (see Methods for the preparation of all DIW inks for use), the resultant DIW ink (Figure 1b) is endowed with ideal rheological behaviors for DIW printing: the shear thinning for the smooth extrusion of gel-like DIW inks through the printer and the high G' and τ_γ values for the self-supporting and shape retention after printing. The DIW printing, aided by

DOI: 10.1021/acsnano.9b06144
ACS Nano 2019, 13, 13176−13184

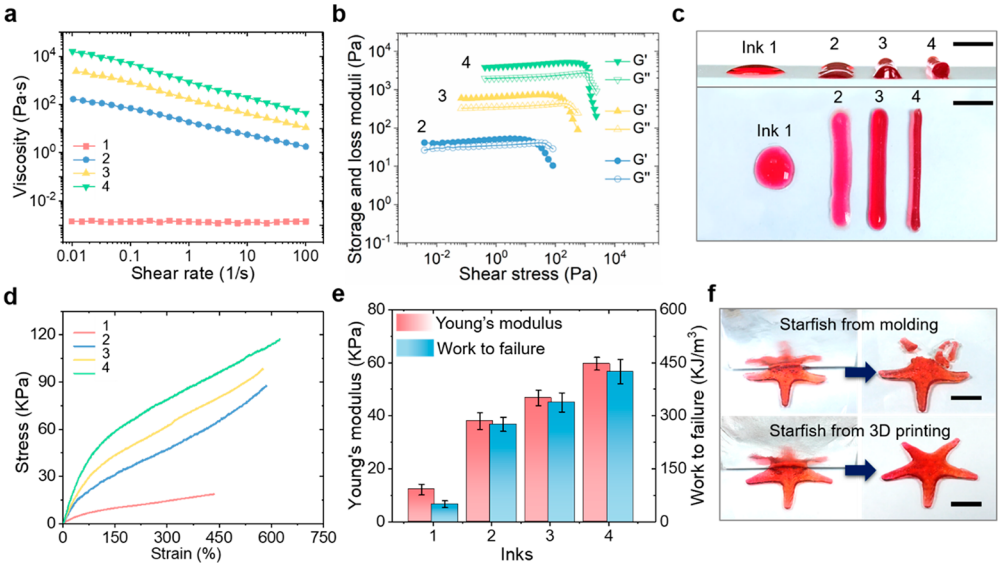

Figure 2. Rheological tuning of DIW inks and mechanical enhancement characterization. (a) Apparent viscosity as a function of shear rate of inks 1−4. (b) Shear storage and loss moduli as a function of shear stress of inks 2−4. (c) Top (bottom) and side (top) views of manually printed lines from inks 1−4 using a syringe (nozzle diameter of 1.8 mm). Scale bars are 10 and 5 mm for bottom and top, respectively. (d) Tensile stress *versus* strain curves of hydrogel samples from inks 1−4. (e) Measured Young's modulus and work-to-failure extracted from (d). (f) Crushing tests on a starfish made from ink 1 through mold-cast (top) and a starfish printed from ink 4 (bottom). Ink 1 is water-like fluid, and mold-cast method is used for the sample preparation. In the test, a metal block (7.6 kg) was loaded on the starfish for 10 s. The starfish from ink 1 broke, and the starfish from ink 4 stayed intact. Scale bars are 2 cm.

a compatible support printing which utilizes pure alginate ink (see Figure S1 for details), gives sophisticated 3D structures from digital design (Figure 1c). The subsequent curing (see Methods for curing conditions for different DIW inks) completes the gelation of the precursor hydrogels. This strategy proved to be highly versatile to hydrogels formed from both chemical bonding and physical entanglement. Printed hydrogels including chemical hydrogels from acrylamide (AAM), acrylic acid (AA), and *N*-isopropylacrylamide (NIPAM), and physical hydrogels from PVA and gelatin are shown in Figure S2. This manufacturing concept is representatively depicted by making a soft and tough starfish from AAM precursor solution (Movie S1). The meticulous integration of the free architectural design and functionality engineering of hydrogels empowers the design of soft robotic systems that can mimic more closely the natural counterparts. Figure 1d demonstrates exemplary prototypes of biomimetic soft robotic systems, including a PAM-based artificial tentacle with 3D mobility, a PVA-based bioengineered robotic heart with beating−transporting functions, and a PNIPAM-based artificial tendril with programmable phototropic motion.

Rheological Tuning and Mechanical Enhancement. Alginate, a natural polysaccharide, is harnessed here as the versatile rheological modifier for the DIW inks, as it possesses high efficiency in regulating viscoelastic properties and also the well-proven biocompatibility, biodegradability, and relatively low cost.[39] To investigate the rheological tailoring effect, we chose AAM as the representative hydrogel precursor, accompanied by the addition of alginate with increasing amounts of 0, 1.7, 3.3, and 6.5 wt %, denoted as inks 1, 2, 3, and 4 in sequence. In Figure 2a, ink 1 (pure AAM solution) shows a constant low η of 1.5 mPa·s, independent of shear rate. The addition of alginate transforms the water-like inks into viscoelastic fluids (inks 2, 3, and 4), suggested by the strong shear thinning behavior, which results in the decreased apparent viscosity along with the increased applied shear rate. This desired shear thinning behavior comes from the mechanically reversible ionic cross-link featuring rapid responsive association/dissociation (detailed information in Figure S3). The η of ink 4 reaches as high as ∼15 600 Pa·s at low shear rate (0.01 s^{-1}) and decreases abruptly to ∼50 Pa·s at a shear rate of 50 s^{-1} (typical value during printing), which is crucial for the consistent flow of DIW inks through the nozzle. In the oscillatory stress sweep testing, inks 2−4 exhibit plateau G' values of 48, 690, and 4650 Pa, respectively, meaning considerably promoted stiffness of the inks with the addition of alginate, as shown in Figure 2b. Also, τ_γ (the crossover point of two moduli curves) for inks 2−4 were measured to be 40, 390, and 2200 Pa, indicating the presence of predominantly elastic networks in inks of higher alginate addition contents. As a comparison, ink 1 (no alginate addition) exhibited constant and much lower values of G' and G'' (Figure S4). The increased G' and τ_γ are in favor of maintaining the designed shape after ink extrusion. To visualize this effect, four straight lines were printed (nozzle size of 1.8 mm) on a glass slide using inks 1−4, as seen in Figure 2c. Ink 1 instantly shrank into a droplet due to the surface tension and gravitational sagging, and inks 2−4 revealed an increased degree of filament shape fidelity, as higher levels of G' and τ_γ help better defy the surface tension and the gravity-driven sagging.

Mechanical performance unquestionably affects the practicality of hydrogel-based soft robots. We performed tensile testing on four cured filamentary samples from inks 1−4 (diameter of 1.5 mm; see Methods for detailed preparation and testing). Figure 2d displays the tensile stress−strain curves, with Young's modulus and work-to-failure results extracted and shown in Figure 2e. Clearly, the Young's moduli and work-to-failure of hydrogels from inks 2−4 reveal significant improvement compared with those of hydrogel from ink 1. Specifically, ink 4 shows a 4-fold increase in Young's modulus (59.6 KPa)

DOI: 10.1021/acsnano.9b06144
ACS Nano 2019, 13, 13176−13184

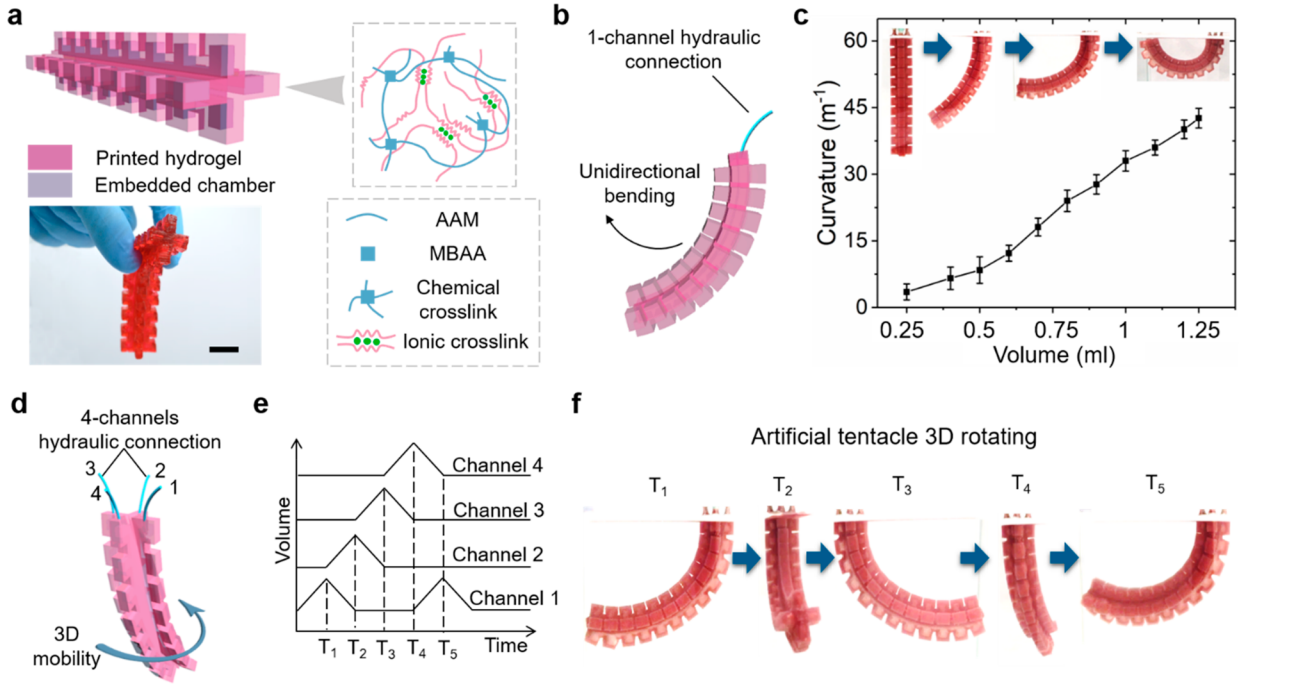

Figure 3. Artificial tentacle with 3D mobility. (a) Designed artificial tentacle structure with the composition diagram and the DIW 3D-printed tentacle photo. Scale bar in the artificial tentacle photo is 10 mm. (b) Schematic diagram of unidirectional bending of the artificial tentacle with one-channel hydraulic connection and (c) bending curvature increase with the injected water volume. The inset photos show the unidirectional bending process, with injection volume being 0, 0.7, 0.9, and 1.25 mL. (d) Schematic diagram of the artificial tentacle with four-channel hydraulic connection to enable 3D mobility. (e) Programmed time-dependent water injection of the four channels and (f) corresponding motion of the artificial tentacle along with time from T_1 to T_5. The artificial tentacle exhibits a full circle rotation. The peak injection volume is 0.8 mL, and one injection cycle time (from T_1 to T_3) is 5.5 s.

and a 7.5-fold increase in work-to-failure (424.6 KJ·m^{-3}), proving that the introduction of the reversible ionic-cross-linking network serves to enhance the mechanical strength and toughness of the resultant hydrogels. The mechanical enhancement could be attributed to the synergy of two mechanisms: crack bridging by the AAM-based covalent network and hysteresis by unzipping the alginate-based ionic cross-links.[40] Figure 2f and Movie S2 vividly show such toughness improvement by performing crushing tests on a starfish made from ink 1 through mold-cast and another starfish directly printed from ink 4. Other hydrogels including PVA, PNIPAM, and PAA also exhibited similar mechanical toughness enhancement with the addition of alginate, as seen in Figure S5.

PAM-Based Hydraulic Artificial Tentacle. Fluidic elastic actuators have gained considerable progress in the applications of biomimetic soft robots,[2,15,30,41−43] due to the facile working principle, easy manipulation, and low power demand. Most of these fluidic elastomer robots either are only capable of simple actuation types or require multiple molding and multistep assembling processes to enrich the complexity of the motion. We here chose PAM hydrogel for the direct construction of a tentacle-like robot with agile 3D mobility, as the covalent bonding nature of PAM polymeric chains offers the prerequisite stretchability and elastic resilience for the reliable operation of fluidic-type actuators.[1,44] The artificial tentacle architecture and the DIW ink composition after curing are shown in Figure 3a. The artificial tentacle features four channels composed of embedded chambers on four sides. The geometric details of the artificial tentacle and its DIW printing aided by support printing are shown in Figure S6. The tests of the robotic performance were implemented under water to counteract the force of gravity. For the one-channel hydraulic connection (Figure 3b), water was injected into one side of the channel and inflated the chambers, resulting in the expansion of the surrounding hydrogel walls. Such asymmetric extension drives the unidirectional bending to the opposite direction of the inflated channel. The bending degree could be controlled through the injected water volume. Figure 3c shows the bending curvature of the artificial tentacle increases with the water volume. As the volume increases from 0.7 to 1.25 mL, the curvature increases from 18 to 42.6 m^{-1}. Next, all four channels were connected to four independently programmable syringe pumps (see Methods for detailed hydraulic actuation information). When two channels in diagonal directions were employed, conceivably the artificial tentacle exhibited corresponding in-plane bending motions, as seen in Figure S7 and Movie S3. Further, when we programmed the four channels collaboratively, the artificial tentacle was capable of generating complex 3D motions (Figure 3d). In Figure 3e, programming the time-dependent output of injected water volume from four syringe pump channels cooperatively drove the artificial tentacle to run a full circle rotation movement (Figure 3f and Movie S4). The smooth 3D mobility originates from the rational incorporation of the multichannel architecture and the intrinsic stretchability of PAM hydrogels.

PVA-Based Bioengineered Robotic Heart. Intense research efforts have been devoted to soft robots that can mimic or assist in biological functions for biomedical applications.[20,45−47] Hydrogel materials hold great promise in this area as a result of their high water content, biocompatibility, permeability of solute, and similar compliance to human

DOI: 10.1021/acsnano.9b06144
ACS Nano 2019, 13, 13176−13184

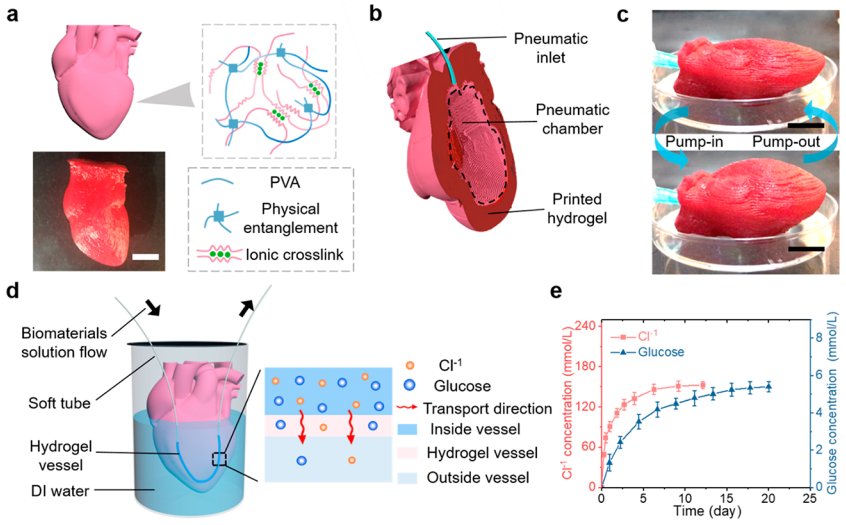

Figure 4. Bioengineered robotic heart with beating−transporting functions. (a) Anatomical heart model with the composition diagram and the DIW 3D-printed PVA-based heart photo (the printed heart size was scaled down to ∼1/3 of the average human heart size). Scale bar in the printed heart is 1 cm. (b) Cross section of the 3D-printed heart model. A pneumatic chamber (indicated by dotted line) is embedded within the heart. A pneumatic inlet was used for the pumping of the robotic heart. (c) Pneumatic pumping drives the beating of the bioengineered robotic heart. Photos show the expansion (bottom photo) of the heart after compressed air was pumped in and contraction (top photo) after pumped out. Scale bars are 1 cm. (d) Schematic setup for the transport test (left) and the schematic diagram (right) of the biomaterial transport from inside the hydrogel vessel to the surrounding DI water environment. (e) Concentration variation of Cl^- and glucose in the DI water along with prolonged time.

tissues.[3,48] PVA, a frequent choice in biomedical uses,[49−51] is employed here to build a bioengineered robotic heart. Figure 4a shows the anatomical human heart model for DIW 3D printing and the corresponding printed PVA-based robotic heart. For the imitation of human heart beating, an embedded chamber was designed in the robotic heart, as shown in the cross section of the 3D printing heart model (Figure 4b). Figure 4c displays that the robotic heart expanded when compressed air was pumped in (bottom photo) and contracted back when pumped out (top photo). The robotic heart also demonstrated continuous heartbeat-like motion when cyclic pneumatic pumping was implemented, as seen in Movie S5.

The transport of fluid for nourishment through the vascular system is another vital functionality for human tissues and organs. To mimic such a function, we used the PVA-based DIW ink to construct microchannel structures with tunable channel size through direct printing. A representative microchannel (square-shaped cross section with a side length of ∼0.7 mm) as a hydrogel vessel was further printed on the outer surface of the heart (see Figure S8 for detailed microchannel geometry and size control). Figure 4d (left) shows the schematic setup for the test of biomaterials transport (see Methods for detailed testing parameters). The solution of sodium chloride and glucose, two typical biomaterials in human blood, was pumped to flow through the microchannel of the hydrogel vessel printed on the robotic heart continuously, and the bioengineered robotic heart was soaked in deionized (DI) water. The porous network of the printed PVA-based hydrogel (SEM characterization in Figure S9) perfused with high water content allows the permeation of water-soluble biomaterials, resulting in their transport from inside the microchannel to the surrounding DI water environment through a combination of convection and concentration gradient-driven diffusion, as shown schematically in Figure 4d (right). The concentrations of Cl^- and glucose in the surrounding DI water were monitored with prolonged time and are displayed in Figure 4e. After 4 and 12 days, the concentrations of Cl^- and glucose reached 90% of the levels in the pumped solution, confirming the effective biomaterial transport function of the hydrogel vessel for the robotic heart. Such a bioengineered robotic heart holds application potentials as a body-part simulator for medical training purposes and even artificial organs with further optimization.[52]

PNIPAM-Based Artificial Tendril. The shape-morphing capability upon desired stimuli has made hydrogels popular in the design of responsive actuators.[23,53,54] DIW 3D printing enables the well-controlled distribution of active hydrogel components, thereby providing the encoding of spatiotemporal response into the final architecture, which resembles the smart movements of a plant tendril. As a specialized stem for climbing plants, tendrils can bend to the surrounding environment and cling to the touched target by forming a helical anchor for competitive growth.[55] Inspired by this natural robotic performance, we devised an artificial tendril capable of programmable phototropic motion for searching and anchoring.

First, a NIPAM-based photoresponsive DIW ink was developed to permit its printing and integration with polydimethylsiloxane (PDMS) substrate (Figure 5a), wherein a multiwalled carbon nanotube (MWCNT) serves as the photothermal element, and a silane coupling agent provides the robust interface bonding between the printed PNIPAM hydrogel and PDMS[56] (for more details, see Figure S10). Due to the temperature-sensitive phase transition of PNIPAM, the hydrogel printed from the DIW ink exhibited a lower critical transition temperature (LCST) of ∼31 °C and a linear contraction ratio of 23% upon the temperature increase to above 40 °C (see Figure S11 for detailed test results). Consequently, the asymmetric thermal responsiveness of the

DOI: 10.1021/acsnano.9b06144
ACS Nano 2019, 13, 13176−13184

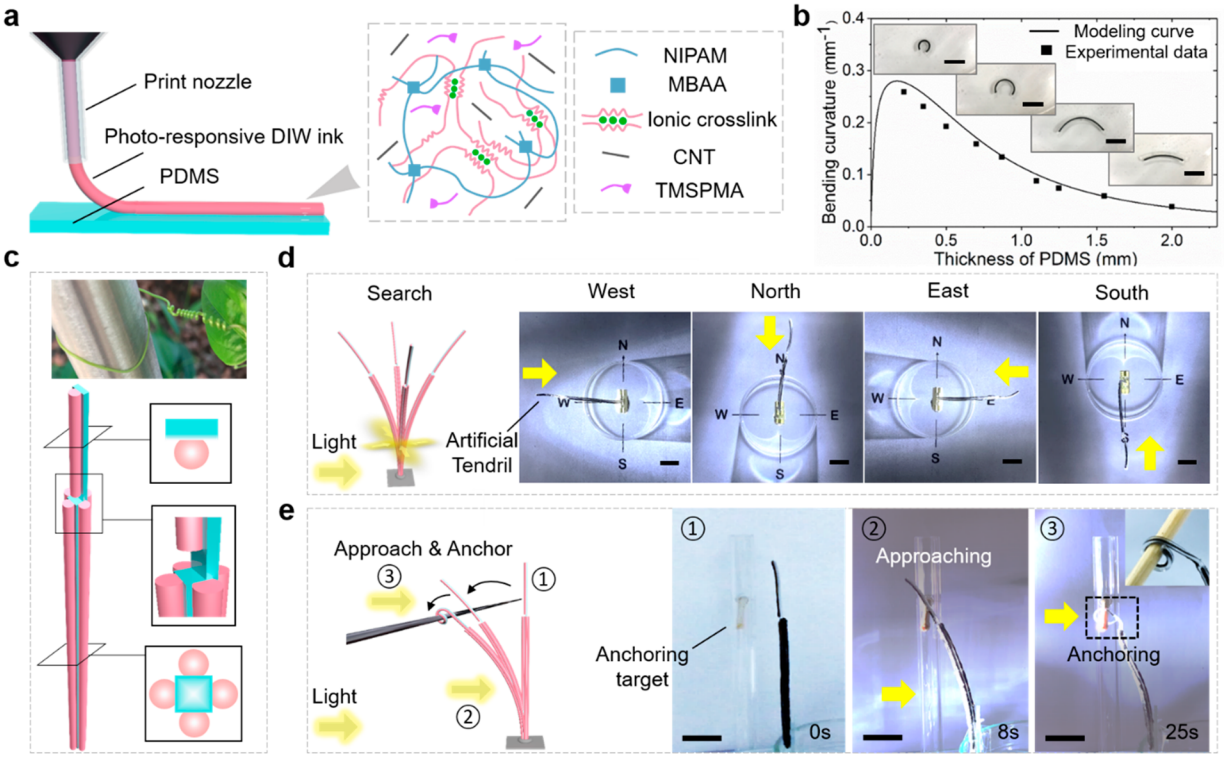

Figure 5. Artificial tendril with programmable phototropic motion. (a) Printing of NIPAM-based DIW ink (schematic) and the composition diagram. (b) Bending curvature of a PNIPAM−PDMS structure upon temperature increase to above 40 °C *versus* the increase of PDMS thickness. Inset photos show the bending of tested samples with PDMS thickness of 0.2, 0.7, 1.25, and 2 mm. Scale bars are all 10 mm. (c) Plant tendril bends and anchors to a target stick (top photo) and the architecture design of the artificial tendril (bottom photo). (d) Artificial tendril showed the searching behavior: bending to the light source direction upon the light irradiation. A xenon lamp with 10 sun intensity was employed to illuminate the artificial tendril (distance of 30 cm) in directions of west, north, east, and south. Scale bars are all 2 cm. (e) Artificial tendril showed the anchoring behavior: approaching and then anchoring to a target (a wooden stick) upon light irradiation moving from the base part to the tip part. A xenon lamp with 10 sun intensity was employed to illuminate the artificial tendril (distance of 30 cm) at the base part and the tip part successively. Scale bars are all 1 cm.

PNIPAM−PDMS bilayer structure would adopt a bending deformation under a temperature increase across the LCST. For a predetermined printing nozzle size (0.84 mm), the bending curvature decreased from 0.26 to 0.04 mm^{-1} as the thickness of the PDMS increased from 0.2 to 2 mm, as seen in Figure 5b and Figure S12. The experimental results conform well to the modeling curve (see section S1 for detailed modeling analysis), thus providing a design rule for more complicated structures.

Figure 5c depicts the architecture design of the artificial tendril, which includes a tip part of the PNIPAM−PDMS bilayer strip and a base part of a square strip with PNIPAM bonding on four sides (see the Methods for the printing process and Figure S13 for the geometric details). When simulated solar light illuminates the artificial tendril at the base part from one direction, the photothermal effect of MWCNTs heats up the corresponding side of printed PNIPAM and resultantly drives the tendril to bend to the light. Figure 5d displayed that the artificial tendril bent toward the light source direction for searching when irradiated from west, north, east, and south (Movie S6). Furthermore, a rotating light direction led to a rotational bending motion of the artificial tendril (Movie S7), similar to the circumnutating motion of plant tendril. Figure 5e demonstrated that, under successive light irradiation to the base part and the tip part, the artificial tendril approached the target and then anchored to it by curling up (Movie S8). The remote and soft manipulation for tendril mimicry functions benefits from the fusion of hydrogel-based responsiveness and the elegant structure enabled by DIW 3D printing.

CONCLUSIONS

We proposed a versatile design and manufacturing platform for directly printing hydrogel materials of chemical and physical types into biomimetic soft robots. The key of this strategy lies in the introduction of an ionic cross-linking network into the functional hydrogel precursors of interest, to enable the rheological tuning for printing and also the accompanied enhancement of mechanical toughness. In this way, we realize the free merging of sophisticated architectures and abundant functionalities from a hydrogel library, which endows us with an avenue to the free design of hydrogel-based biomimetic soft robots. As a proof of concept, we demonstrated an artificial tentacle with 3D mobility, a bioengineered robotic heart capable of beating and transporting biomaterials, and an artificial tendril with programmable phototropic motion. Apart from the individual architecture design of these robots, the biomimetic robotic functions stem from the properties of these target hydrogels, like stretchability, permeability, and stimuli-responsiveness.

The blending of the ionic-cross-linking network into a covalently cross-linked hydrogel has already been put forward for improving the mechanical toughness of the resultant hydrogels and proved to be highly effective.[40] In this work, we

DOI: 10.1021/acsnano.9b06144
ACS Nano 2019, 13, 13176−13184

further explored the rheological tuning behavior of the alginate-based modifier and leveraged the tailoring rule to extend the exploitable hydrogel precursor system types from pourable to printable. More importantly, the versatility of this strategy was also confirmed for both chemically and physically cross-linked hydrogels. With the advancement in both 3D printing techniques and the engineering of hydrogel materials, such a design concept holds great promise to be broadened to other application fields, such as hydrogel-based wearable electronics, human-friendly sensors, and biomedical therapeutics.

METHODS

DIW Ink Preparation. For AAM-based DIW ink, we dissolved 1 g of AAM (TCI, A0139) as monomer, 6 mg of *N*,*N*′-methylenebis-(acrylamide) (MBAA, TCI, M2877) as cross-linker, and 8 mg of ammonium persulfate (APS, TCI, A2098) as radical initiator in every 10 mL of distilled water and denoted this recipe as AAM-based DIW ink 1. Further, a pair of sodium alginate (Sigma-Aldrich, 180947) and calcium chloride (Sigma-Aldrich, C1016) were added into AAM-based DIW ink 1, with contents of 1.7 and 0.1 wt % as DIW ink 2, 3.3 and 0.2 wt % as DIW ink 3, and 6.5 and 0.4 wt % as DIW ink 4. For AA-based DIW ink, we dissolved 1 g of AA (Sigma-Aldrich, 147230) as monomer, 5 mg of MBAA as cross-linker, 10 mg of APS as radical initiator, sodium alginate of 6 wt % and calcium chloride of 0.4 wt % as rheological modifier in every 10 mL of distilled water. For NIPAM-based DIW ink, we dissolved 1 g of NIPAM (TCI, I0401) as monomer, 6 mg of MBAA as cross-linker, 10 mg of 2,2-diethoxyacetophenone (TCI, D1640) as photoinitiator, and sodium alginate of 6 wt % and calcium chloride of 0.4 wt % as rheological modifiers in every 10 mL of distilled water. For photoresponsive NIPAM-based DIW ink, an extra 0.3 g of MWCNT (XFNANO, XFM03) solution (0.34 wt % in distilled water) as photothermal element and 10 mg of 3-(trimethoxysilyl)propyl methacrylate (TMSPMA, TCI, M0725) as silane coupling agent were added in 10 mL of the aforementioned NIPAM-based DIW ink. For PVA-based DIW ink, we dissolved 0.75 g of PVA (Sigma-Aldrich, 341584) as precursor and sodium alginate of 4 wt % and calcium chloride of 0.25 wt % as rheological modifiers in every 10 mL of distilled water. For gelatin-based DIW ink, we dissolved 0.5 g of gelatin powder (REDMAN, 160BLOOM) as precursor and sodium alginate of 4 wt % and calcium chloride of 0.25 wt % as rheological modifiers in every 10 mL of distilled water. For the precursor of PDMS, the base and curing agent of Sylgard 184 (Dow Corning) at a 10:1 weight ratio was mixed, and then triethoxyvinylsilane (TEOVS, TCI, V0044) as a silane coupling agent of 1.5 wt % was added. Trace amount of red food dye (0.1 wt %) can be added into the above DIW inks to visualize the printed shapes. To fully dissolve the sodium alginate, vigorous stirring was needed using a spatula. To fully dissolve PVA and gelatin, the solution was first heated to ∼80 °C and then cooled for the addition of sodium alginate. All the DIW inks were centrifuged to remove bubbles before being loaded to a 3D printer (5axismaker 5xm400).

Curing Conditions. For the curing of AAM-, AA-, and NIPAM-based DIW ink, the printed samples were kept in a sealed chamber with humid nitrogen atmosphere and irradiated by UV light (365 nm) for 10 min. An ice−water bath was used in the curing process of NIPAM-based hydrogel. For the curing of PVA-based DIW ink, the printed samples were exposed to five cycles of freezing for 8 h at −20 °C and thawing for 4 h at 25 °C. For the curing of gelatin-based DIW ink, the printed samples were cooled to 4 °C for 24 h.

Rheology Test. All of the DIW inks were centrifuged to remove bubbles prior to rheological characterization. A MCR302 rheometer (Anton Paar) with cone−plate geometry was used for tests at 22 °C. Viscometry measurements were carried out over shear rates ranging from 0.01 to 100 s^{-1}. Oscillatory amplitude sweeps were performed at 1 Hz within strain values from 0.01 to 100%.

Mechanical Test and Sample Preparation. For preparation of testing samples, a hollow polytetrafluoroethylene tube with an inner diameter of 1.6 mm was used as the template. Inks 1−4 were injected into the tube template using a syringe. After UV irradiation, the cured hydrogel filament (4 cm in length) was extruded out of the template for mechanical tests. The tensile stress−strain test was implemented using a customized setup: 1 lb force gauge was mounted on a high-precision step motor. The response from the force gauge is amplified using a 24 bit load cell amplifier (SparkFun, HX711) and logged using an Arduino.

Hydraulic Actuation Test. The four channels of the artificial tentacle were connected to four independent syringe pumps (LEGATO270P, KDScientific) with programmable output assisted by computers. The air bubbles within the chambers of the artificial tentacle were removed by degassing before actuation. Pressurized water from the syringe pumps were injected into the tentacle channels through connections of metallic needles and silicone tubes. The unidirectional bending of the artificial tentacle was performed by infusion and withdrawal of water using a channel. The in-plane bending was performed by the infusion and withdrawal of water using two channels in a diagonal direction. The 3D rotation was performed by the synchronous and programmable control of four channels. The output force of the artificial tentacle during actuation was also tested, as seen in Figure S14.

Biomaterial Transport Test. The bioengineered robotic heart was soaked in DI water for 24 h to reach swelling equilibrium. A solution of sodium chloride (Fisher Chemical, S/3161/60) and glucose (Sigma-Aldrich, G8270) was prepared with concentrations of 154 and 5.5 mmol/L, respectively, similar to the average levels in human blood. The prepared solution was pumped by a syringe pump to flow through the microchannel on the bioengineered robotic heart at a rate of 1 mL/h by using metallic needles and silicone tubes for connection. At the same time, the robotic heart was put in a container with 40 mL of DI water, and the hydrogel vessel was immersed in the water. The concentrations of Cl^- and glucose in the container were monitored using an ion meter (Thermo Scientific, Orion Star A214) and a glucose meter. To avoid water evaporation, the container was sealed with plastic wrap.

Printing of the Artificial Tendril. To enable the printing of photoresponsive NIPAM-based DIW ink on four sides of the PDMS strip, a customized rotational gripper was used to fix the PDMS strip and rotate as required during the printing. The interfacial adhesion strength between PDMS and NIPAM-based DIW ink was high enough to maintain the bonding in the rotation process. Lap shear test for the evaluation of the adhesion strength of the PNIPAM-based inks is shown in Figure S15. After being printed, the artificial tendril was irradiated by UV light (10 min) for curing and then kept in a sealed chamber for 1 day to allow the interface bonding reaction of silane coupling agents (the detailed chemical process in Figure S16).

ASSOCIATED CONTENT

Supporting Information

The Supporting Information is available free of charge on the ACS Publications website at DOI: 10.1021/acsnano.9b06144.

Movie S1: DIW 3D printing of a starfish (MP4)

Movie S2: Mechanical toughness comparison (MP4)

Movie S3: In-plane bending of an artificial tentacle (MP4)

Movie S4: 3D mobility of an artificial tentacle (MP4)

Movie S5: Robotic heartbeat (MP4)

Movie S6: Artificial tendril bending (MP4)

Movie S7: Artificial tendril anchoring (MP4)

Movie S8: Artificial tendril circumnutating (MP4)

Bending curvature analysis; Figures S1−S10 (PDF)

DOI: 10.1021/acsnano.9b06144
ACS Nano 2019, 13, 13176−13184

AUTHOR INFORMATION

Corresponding Author

*E-mail: elehgw@nus.edu.sg.

ORCID

Ghim Wei Ho: 0000-0003-1276-0165

Notes

The authors declare no competing financial interest.

ACKNOWLEDGMENTS

This research is supported by the Singapore Ministry of National Development and the National Research Foundation, Prime Minister's Office under the Land and Liveability National Innovation Challenge (L2 NIC) Research Programme (L2 NIC Award No. L2NICCFP2-2015-3) and R-263-501-011-731.

REFERENCES

(1) Rus, D.; Tolley, M. T. Design, Fabrication and Control of Soft Robots. *Nature* **2015**, *521*, 467−475.

(2) Shepherd, R. F.; Ilievski, F.; Choi, W.; Morin, S. A.; Stokes, A. A.; Mazzeo, A. D.; Chen, X.; Wang, M.; Whitesides, G. M. Multigait Soft Robot. *Proc. Natl. Acad. Sci. U. S. A.* **2011**, *108*, 20400−20403.

(3) Lu, H.; Zhang, M.; Yang, Y.; Huang, Q.; Fukuda, T.; Wang, Z.; Shen, Y. A Bioinspired Multilegged Soft Millirobot That Functions in Both Dry and Wet Conditions. *Nat. Commun.* **2018**, *9*, 3944.

(4) Bartlett, N. W.; Tolley, M. T.; Overvelde, J. T. B.; Weaver, J. C.; Mosadegh, B.; Bertoldi, K.; Whitesides, G. M.; Wood, R. J. A 3D-Printed, Functionally Graded Soft Robot Powered by Combustion. *Science* **2015**, *349*, 161.

(5) Cheng, Y.; Wang, R.; Chan, K. H.; Lu, X.; Sun, J.; Ho, G. W. A Biomimetic Conductive Tendril for Ultrastretchable and Integratable Electronics, Muscles, and Sensors. *ACS Nano* **2018**, *12*, 3898−3907.

(6) Zhu, L.; Cao, Y.; Liu, Y.; Yang, Z.; Chen, X. Architectures of Soft Robotic Locomotion Enabled by Simple Mechanical Principles. *Soft Matter* **2017**, *13*, 4441−4456.

(7) Cheng, Y.; Lu, X.; Chan, K. H.; Wang, R.; Cao, Z.; Sun, J.; Ho, G. W. A Stretchable Fiber Nanogenerator for Versatile Mechanical Energy Harvesting and Self-Powered Full-Range Personal Healthcare Monitoring. *Nano Energy* **2017**, *41*, 511−518.

(8) Li, K.; Shao, Y.; Yan, H.; Lu, Z.; Griffith, K. J.; Yan, J.; Wang, G.; Fan, H.; Lu, J.; Huang, W.; Bao, B.; Liu, X.; Hou, C.; Zhang, Q.; Li, Y.; Yu, J.; Wang, H. Lattice-Contraction Triggered Synchronous Electrochromic Actuator. *Nat. Commun.* **2018**, *9*, 4798.

(9) Wang, X.-Q.; Tan, C. F.; Chan, K. H.; Lu, X.; Zhu, L.; Kim, S.-W.; Ho, G. W. In-Built Thermo-Mechanical Cooperative Feedback Mechanism for Self-Propelled Multimodal Locomotion and Electricity Generation. *Nat. Commun.* **2018**, *9*, 3438.

(10) Wani, O. M.; Zeng, H.; Priimagi, A. A Light-Driven Artificial Flytrap. *Nat. Commun.* **2017**, *8*, 15546.

(11) Wani, O. M.; Verpaalen, R.; Zeng, H.; Priimagi, A.; Schenning, A. An Artificial Nocturnal Flower *via* Humidity-Gated Photoactuation in Liquid Crystal Networks. *Adv. Mater.* **2019**, *31*, 1805985.

(12) Park, S.-J.; Gazzola, M.; Park, K. S.; Park, S.; Di Santo, V.; Blevins, E. L.; Lind, J. U.; Campbell, P. H.; Dauth, S.; Capulli, A. K.; Pasqualini, F. S.; Ahn, S.; Cho, A.; Yuan, H.; Maoz, B. M.; Vijaykumar, R.; Choi, J.-W.; Deisseroth, K.; Lauder, G. V.; Mahadevan, L.; et al. Phototactic Guidance of a Tissue-Engineered Soft-Robotic Ray. *Science* **2016**, *353*, 158.

(13) Li, T.; Li, G.; Liang, Y.; Cheng, T.; Dai, J.; Yang, X.; Liu, B.; Zeng, Z.; Huang, Z.; Luo, Y.; Xie, T.; Yang, W. Fast-Moving Soft Electronic Fish. *Sci. Adv.* **2017**, *3*, e1602045.

(14) Ionov, L. Biomimetic Hydrogel-Based Actuating Systems. *Adv. Funct. Mater.* **2013**, *23*, 4555−4570.

(15) Yuk, H.; Lin, S.; Ma, C.; Takaffoli, M.; Fang, N. X.; Zhao, X. Hydraulic Hydrogel Actuators and Robots Optically and Sonically Camouflaged in Water. *Nat. Commun.* **2017**, *8*, 14230.

(16) Jiang, S.; Liu, F.; Lerch, A.; Ionov, L.; Agarwal, S. Unusual and Superfast Temperature-Triggered Actuators. *Adv. Mater.* **2015**, *27*, 4865−4870.

(17) Peng, X.; Li, Y.; Zhang, Q.; Shang, C.; Bai, Q.-W.; Wang, H. Tough Hydrogels with Programmable and Complex Shape Deformations by Ion Dip-Dyeing and Transfer Printing. *Adv. Funct. Mater.* **2016**, *26*, 4491−4500.

(18) Shi, Y.; Ma, C.; Peng, L.; Yu, G. Conductive "Smart" Hybrid Hydrogels with Pnipam and Nanostructured Conductive Polymers. *Adv. Funct. Mater.* **2015**, *25*, 1219−1225.

(19) Zheng, J.; Xiao, P.; Le, X.; Lu, W.; Théato, P.; Ma, C.; Du, B.; Zhang, J.; Huang, Y.; Chen, T. Mimosa Inspired Bilayer Hydrogel Actuator Functioning in Multi-Environments. *J. Mater. Chem. C* **2018**, *6*, 1320−1327.

(20) Roche, E. T.; Horvath, M. A.; Wamala, I.; Alazmani, A.; Song, S.-E.; Whyte, W.; Machaidze, Z.; Payne, C. J.; Weaver, J. C.; Fishbein, G.; Kuebler, J.; Vasilyev, N. V.; Mooney, D. J.; Pigula, F. A.; Walsh, C. J. Soft Robotic Sleeve Supports Heart Function. *Sci. Transl. Med.* **2017**, *9*, eaaf3925.

(21) Yang, B.; Yao, C.; Yu, Y.; Li, Z.; Wang, X. Nature Degradable, Flexible, and Transparent Conductive Substrates from Green and Earth-Abundant Materials. *Sci. Rep.* **2017**, *7*, 4936.

(22) Yang, C.; Liu, Z.; Chen, C.; Shi, K.; Zhang, L.; Ju, X. J.; Wang, W.; Xie, R.; Chu, L. Y. Reduced Graphene Oxide-Containing Smart Hydrogels with Excellent Electro-Response and Mechanical Properties for Soft Actuators. *ACS Appl. Mater. Interfaces* **2017**, *9*, 15758−15767.

(23) Palleau, E.; Morales, D.; Dickey, M. D.; Velev, O. D. Reversible Patterning and Actuation of Hydrogels by Electrically Assisted Ionoprinting. *Nat. Commun.* **2013**, *4*, 2257.

(24) Xie, W.; Duan, J.; Wang, H.; Li, J.; Liu, R.; Yu, B.; Liu, S.; Zhou, J. Ultra-Stretchable, Bio-Inspired Ionic Skins That Work Stably in Various Harsh Environments. *J. Mater. Chem. A* **2018**, *6*, 24114−24119.

(25) Calvert, P. Hydrogels for Soft Machines. *Adv. Mater.* **2009**, *21*, 743−756.

(26) Fuhrer, R.; Athanassiou, E. K.; Luechinger, N. A.; Stark, W. J. Crosslinking Metal Nanoparticles into the Polymer Backbone of Hydrogels Enables Preparation of Soft, Magnetic Field-Driven Actuators with Muscle-Like Flexibility. *Small* **2009**, *5*, 383−388.

(27) Yu, C.; Duan, Z.; Yuan, P.; Li, Y.; Su, Y.; Zhang, X.; Pan, Y.; Dai, L. L.; Nuzzo, R. G.; Huang, Y.; Jiang, H.; Rogers, J. A. Electronically Programmable, Reversible Shape Change in Two- and Three-Dimensional Hydrogel Structures. *Adv. Mater.* **2013**, *25*, 1541−1546.

(28) Lee, B. P.; Konst, S. Novel Hydrogel Actuator Inspired by Reversible Mussel Adhesive Protein Chemistry. *Adv. Mater.* **2014**, *26*, 3415−3419.

(29) Peng, X.; Liu, T.; Jiao, C.; Wu, Y.; Chen, N.; Wang, H. Complex Shape Deformations of Homogeneous Poly(N-Isopropylacrylamide)/Graphene Oxide Hydrogels Programmed by Local Nir Irradiation. *J. Mater. Chem. B* **2017**, *5*, 7997−8003.

(30) Mosadegh, B.; Polygerinos, P.; Keplinger, C.; Wennstedt, S.; Shepherd, R. F.; Gupta, U.; Shim, J.; Bertoldi, K.; Walsh, C. J.; Whitesides, G. M. Pneumatic Networks for Soft Robotics That Actuate Rapidly. *Adv. Funct. Mater.* **2014**, *24*, 2163−2170.

(31) Parida, K.; Thangavel, G.; Cai, G.; Zhou, X.; Park, S.; Xiong, J.; Lee, P. S. Extremely Stretchable and Self-Healing Conductor Based on Thermoplastic Elastomer for All-Three-Dimensional Printed Triboelectric Nanogenerator. *Nat. Commun.* **2019**, *10*, 2158.

(32) Ouyang, L.; Highley, C. B.; Sun, W.; Burdick, J. A. A Generalizable Strategy for the 3D Bioprinting of Hydrogels from Nonviscous Photo-Crosslinkable Inks. *Adv. Mater.* **2017**, *29*, 1604983.

(33) Tian, K.; Bae, J.; Bakarich, S. E.; Yang, C.; Gately, R. D.; Spinks, G. M.; Het Panhuis, M.; Suo, Z.; Vlassak, J. J. 3D Printing of Transparent and Conductive Heterogeneous Hydrogel-Elastomer Systems. *Adv. Mater.* **2017**, *29*, 1604827.

(34) Hong, S.; Sycks, D.; Chan, H. F.; Lin, S.; Lopez, G. P.; Guilak, F.; Leong, K. W.; Zhao, X. 3D Printing of Highly Stretchable and

DOI: 10.1021/acsnano.9b06144
ACS Nano 2019, 13, 13176−13184

Tough Hydrogels into Complex, Cellularized Structures. *Adv. Mater.* **2015**, *27*, 4035−4040.
(35) Odent, J.; Wallin, T. J.; Pan, W.; Kruemplestaedter, K.; Shepherd, R. F.; Giannelis, E. P. Highly Elastic, Transparent, and Conductive 3D-Printed Ionic Composite Hydrogels. *Adv. Funct. Mater.* **2017**, *27*, 1701807.
(36) Zhai, X.; Ma, Y.; Hou, C.; Gao, F.; Zhang, Y.; Ruan, C.; Pan, H.; Lu, W. W.; Liu, W. 3D-Printed High Strength Bioactive Supramolecular Polymer/Clay Nanocomposite Hydrogel Scaffold for Bone Regeneration. *ACS Biomater. Sci. Eng.* **2017**, *3*, 1109−1118.
(37) Schaffner, M.; Rühs, P. A.; Coulter, F.; Kilcher, S.; Studart, A. R. 3D Printing of Bacteria into Functional Complex Materials. *Sci. Adv.* **2017**, *3*, eaao6804.
(38) Jin, Y.; Liu, C.; Chai, W.; Compaan, A.; Huang, Y. Self-Supporting Nanoclay as Internal Scaffold Material for Direct Printing of Soft Hydrogel Composite Structures in Air. *ACS Appl. Mater. Interfaces* **2017**, *9*, 17456−17465.
(39) Lee, K. Y.; Mooney, D. J. Alginate: Properties and Biomedical Applications. *Prog. Polym. Sci.* **2012**, *37*, 106−126.
(40) Sun, J. Y.; Zhao, X.; Illeperuma, W. R.; Chaudhuri, O.; Oh, K. H.; Mooney, D. J.; Vlassak, J. J.; Suo, Z. Highly Stretchable and Tough Hydrogels. *Nature* **2012**, *489*, 133−136.
(41) Terryn, S.; Brancart, J.; Lefeber, D.; Van Assche, G.; Vanderborght, B. Self-Healing Soft Pneumatic Robots. *Sci. Robot.* **2017**, *2*, eaan4268.
(42) Marchese, A. D.; Onal, C. D.; Rus, D. Autonomous Soft Robotic Fish Capable of Escape Maneuvers Using Fluidic Elastomer Actuators. *Soft Robot* **2014**, *1*, 75−87.
(43) Martinez, R. V.; Branch, J. L.; Fish, C. R.; Jin, L.; Shepherd, R. F.; Nunes, R. M.; Suo, Z.; Whitesides, G. M. Robotic Tentacles with Three-Dimensional Mobility Based on Flexible Elastomers. *Adv. Mater.* **2013**, *25*, 205−212.
(44) Marchese, A. D.; Katzschmann, R. K.; Rus, D. A Recipe for Soft Fluidic Elastomer Robots. *Soft Robot* **2015**, *2*, 7−25.
(45) Roche, E. T.; Wohlfarth, R.; Overvelde, J. T.; Vasilyev, N. V.; Pigula, F. A.; Mooney, D. J.; Bertoldi, K.; Walsh, C. J. A Bioinspired Soft Actuated Material. *Adv. Mater.* **2014**, *26*, 1200−1206.
(46) Damian, D. D.; Price, K.; Arabagi, S.; Berra, I.; Machaidze, Z.; Manjila, S.; Shimada, S.; Fabozzo, A.; Arnal, G.; Van Story, D.; Goldsmith, J. D.; Agoston, A. T.; Kim, C.; Jennings, R. W.; Ngo, P. D.; Manfredi, M.; Dupont, P. E. *In Vivo* Tissue Regeneration with Robotic Implants. *Sci. Robot.* **2018**, *3*, eaaq0018.
(47) Mac Murray, B. C.; An, X.; Robinson, S. S.; van Meerbeek, I. M.; O'Brien, K. W.; Zhao, H.; Shepherd, R. F. Poroelastic Foams for Simple Fabrication of Complex Soft Robots. *Adv. Mater.* **2015**, *27*, 6334−6340.
(48) Hoffman, A. S. Hydrogels for Biomedical Applications. *Adv. Drug Delivery Rev.* **2012**, *64*, 18−23.
(49) Gonzalez, J. S.; Maiolo, A. S.; Hoppe, C. E.; Alvarez, V. A. Composite Gels Based on Poly (Vinyl Alcohol) for Biomedical Uses. *Procedia Mater. Sci.* **2012**, *1*, 483−490.
(50) Paradossi, G.; Cavalieri, F.; Chiessi, E.; Spagnoli, C.; Cowman, M. K. Poly(Vinyl Alcohol) as Versatile Biomaterial for Potential Biomedical Applications. *J. Mater. Sci.: Mater. Med.* **2003**, *14*, 687−691.
(51) Jiang, S.; Liu, S.; Feng, W. Pva Hydrogel Properties for Biomedical Application. *J. Mech. Behav. Biomed.* **2011**, *4*, 1228−1233.
(52) Cianchetti, M.; Laschi, C.; Menciassi, A.; Dario, P. Biomedical Applications of Soft Robotics. *Nat. Rev. Mater.* **2018**, *3*, 143−153.
(53) Jeon, S. J.; Hauser, A. W.; Hayward, R. C. Shape-Morphing Materials from Stimuli-Responsive Hydrogel Hybrids. *Acc. Chem. Res.* **2017**, *50*, 161−169.
(54) Zhang, X.; Pint, C. L.; Lee, M. H.; Schubert, B. E.; Jamshidi, A.; Takei, K.; Ko, H.; Gillies, A.; Bardhan, R.; Urban, J. J.; Wu, M.; Fearing, R.; Javey, A. Optically- and Thermally-Responsive Programmable Materials Based on Carbon Nanotube-Hydrogel Polymer Composites. *Nano Lett.* **2011**, *11*, 3239−3244.
(55) Isnard, S.; Silk, W. K. Moving with Climbing Plants from Charles Darwin's Time into the 21st Century. *Am. J. Bot.* **2009**, *96*, 1205−1221.
(56) Liu, Q.; Nian, G.; Yang, C.; Qu, S.; Suo, Z. Bonding Dissimilar Polymer Networks in Various Manufacturing Processes. *Nat. Commun.* **2018**, *9*, 846.

DOI: 10.1021/acsnano.9b06144
ACS Nano 2019, 13, 13176−13184